LES STUDIES OF SCALAR FLUCTUATIONS AT HIGH CONVECTIVE MACH NUMBERS

WILLIAM H. CALHOON, JR., CHANDRASEKHAR KANNEPALLI AND SANFORD M. DASH
Combustion Research and Flow Technology, Inc. (CRAFT Tech)
Dublin, PA 18917

Abstract

A need has arisen for the development of RANS models for the prediction of scalar fluctuations and turbulent transport in the high speed flow regime. These models will have application, for example, in scramjet combustors and missile exhaust plume signature analyses and other important areas. However, in the high speed flow regime, experimentally derived scalar fluctuation validation data is not readily available due to the inability of relevant experimental measurement techniques (e.g. hot wires) to cope with this flowfield environment. Consequently, model development in this flow regime is difficult. To address this issue, a two part program has been initiated to fill the data gap and thus facilitate model development. Part I of this program involves the collection of LES data over a wide range of conditions. Part II involves the use of these data to evaluate and develop RANS tools to improve predictive capabilities. This paper presents results and preliminary finding of Part I of this program; the collection of LES data regarding scalar transport in planar shear layers. The findings of this study elucidate the effects of compressibility on the character of mean scalar profiles, variations in turbulent Prandtl number, and on scalar rms fluctuations.

1. Introduction

The ability of LES methodology to predict scalar variance properties for both hot and variable composition jets and free shear layers at subsonic conditions has been amply demonstrated, as exemplified by a number of comparisons with the Brown and Roshko Nitrogen/Helium shear layer density variance data of Konrad (see, e.g. Ref. 1). The time-averaged statistics from these type of simulations, in combination with available subsonic hot jet and helium jet data, have served as the basis for RANS (Reynolds Average Navier-Stokes) scalar variance model equation calibration [2], which are in turn utilized for both variable turbulent Prandtl (Pr_t) and Schmidt (Sc_t) number modeling [3] and for PDF-based turbulent combustion modeling [4].

For supersonic flows with high convective Mach numbers, compressibility effects reduce the rate of mixing and turbulent fluctuation levels. However, while significant data is available for Favre averaged velocity fluctuations at high convective numbers, there is a lack of comparable data for scalar correlations. The lack of data in this flow regime makes the calibration and application of RANS scalar fluctuation models difficult. Recently, Calhoon [4] found that a RANS scalar fluctuation model, which had been calibrated using available low speed data, overpredicted fluctuation levels leading to substantive errors in missile exhaust plume flows. This failure of RANS modeling resulted from a lack of adequate data which could provide an understanding of the effects of compressibility on scalar fluctuations. Available experimental data for scalar fluctuations in this high speed flow regime are not readily available.

LES provides the opportunity to investigate compressibility effects on scalar fluctuations in the high speed flow regime where experimental data are difficult to obtain. Data from LES in this regime could also be used to develop and calibrate RANS models to be applied to large scale problems such as scramjet combustors, rocket plume signatures and missile sensor window aero-optics. Proper understanding of scalar fluctuations in the high speed regime is a prerequisite to the development of reliable turbulent-combustion models for scramjet and rocket propulsive applications.

With these points in mind, the objective of this overall study is to investigate compressibility effects on scalar fluctuations and evaluate RANS modeling for the prediction of these fluctuations. This will be accomplished by conducting LES simulations of hot shear layers at varying degrees of compressibility. The primary scalar fluctuations of interest will be those of temperature. Analysis of the simulation results will enable the assessment of compressibility effects on fluctuation levels and the effect of variable turbulent Prandtl number in these flows. Time-averaged statistics will also be used to evaluate and calibrate RANS models for temperature fluctuations and variable Pr_t.

This study has been broken into two parts. Part I deals with the collection of LES data for shear layers at varying degrees of compressibility. Part II deals with the analysis and use of these data for the development of RANS models for the prediction of scalar fluctuations, and turbulent Prandtl and Schmidt numbers, which accurately characterize compressibility effects. This paper concerns Part I of this study and presents a summary of the LES data that has been collected thus far. Though not complete, the data collected so far does reveal some interesting aspects of compressibility effects on free shear layer development and scalar fluctuations.

The following section briefly describes the computational methodology used for the LES simulations. Next, a description of the simulations carried out for Part I is presented, followed by the presentation and discussion of the results and analysis. Concluding remarks follow.

2. Computational Methodology

The simulations for this study were carried out using the CRAFT NS code [5,6]. CRAFT is a structured, finite-volume code applicable to compressible, reacting, multi-phase flows. For LES applications, the code is implemented with an upwind-biased, Roe-flux-extrapolation procedure extended to fifth order [7] and fourth order central differencing for the inviscid and viscous spatial schemes, respectively. Temporally, the code includes both a fourth order Runga-Kutta scheme and second order three-factor Approximate Factorization (AF) implicit scheme. For this study, the AF scheme was used and applied with sub-iterations to remove the splitting error. Regarding subgrid modeling, the code includes a compressible version of the algebraic Smagorinsky model as well as the compressible, one equation model of Menon [8]. The one equation model solves a transport equation for subgrid turbulent kinetic energy, k^{sgs}. The subgrid-scale stresses are then modeled using an eddy viscosity approach based on k^{sgs}.

For high speed applications where shock waves are present, the higher order numerical scheme requires modification for stability. Shock capturing options for higher order schemes range from standard limiting approaches to WENO schemes (e.g., Ref. [10]). An alternative approach was used in this study. In order to stabilize the code in the vicinity of strong gradients, such as shock waves, a modification of the classic Jameson, *et al.* [11] 2-4 dissipation scheme was used. In the original scheme, a fourth order dissipation term was employed to stabilize the central difference scheme in smooth, high cell Reynolds number regions of the flow. In the vicinity of shocks, a pressure based switch was used to deactivate the fourth order dissipation and turn on a second order dissipation term. In the present context, the fourth order dissipation term is not required and is discarded. The second order dissipation term is retained to provide sufficient stability for the fifth order code in the vicinity of shock waves. The original Jameson second order dissipation term, including the calibration constant, was used with only the following modification. The pressure based switch was modified to also include temperature to prevent instabilities along slip lines. Also, both the pressure and temperature switches were threshold to allow the dissipation to be tuned for shock waves, to ensure no dissipation is added elsewhere. The following form of the second order dissipation switch, ν, was used,

$$\nu = \max(\nu_p, \nu_T) \tag{1}$$

where,

$\nu_p = \frac{|p_{i+1} - 2p_i + p_{i-1}|}{|p_{i+1}| + |2p_i| + |p_{i-1}|}$ and $\nu_T = \frac{|T_{i+1} - 2T_i + T_{i-1}|}{|T_{i+1}| + |2T_i| + |T_{i-1}|}$ with p and T being the pressure and temperature, respectively. These values were then threshold as $\nu_p = 0$ if $\nu_p < \nu_{p,0}$ and $\nu_T = 0$ if $\nu_T < \nu_{T,0}$. Values of the threshold cuts-offs in numerical tests were $\nu_{p,0} = 0.2$ and $\nu_{T,0} = 0.3$. Tests of the scheme were carried out for vortex convection, a shock-vortex interaction, wave propagation, and a supersonic flat plate boundary layer. These tests demonstrated the second order dissipation to be isolated around shock waves and to have no impact on the development of unsteady flow features elsewhere.

3.0 LES Shear Layer Simulation

Sandham and Reynolds [9] found three distinct flow regimes for compressible mixing layers using linear stability analysis and DNS. These flow regimes are characterized by the convective Mach number, M_c, which may be defined as,

$$M_c = \frac{M_1\sqrt{\rho_2/\rho_1}(1-u_2/u_1)}{(\gamma_2/\gamma_1)^{1/4}(1+\sqrt{\rho_2/\rho_1})} \tag{2}$$

where u, M, ρ and γ are the velocity, Mach number, density and ratio of specific heats, respectively, for the high speed (subscript 1) and low speed (subscript 2) sides. For $0 < M_c < 0.6$, two-dimensional instabilities are amplified most rapidly so that the shear layer is dominated by large scale 2-D spanwise structures. For $0.6 < M_c < 1.0$, oblique (three-dimensional) instability modes become dominant while 2-D instabilities are still significantly amplified resulting in a shear layer which is composed of both strong 2-D and 3-D structures. For $M_c > 1.0$, 2-D instabilities are amplified by a factor of five less than 3-D modes resulting in a flow dominated by 3-D large scale structures with little or no organized 2-D structures.

To characterize compressibility effects on the evolution of shear layer scalar fluctuations, simulations for Part I of this study must be carried out in each of these flow regimes. Convective Mach numbers chosen for the study were $M_c = 0.27$, 0.8 and 1.3. Additionally, all the simulations were for spatially evolving shear layers, as opposed to temporally evolving layers. Other numerical studies of spatially evolving compressible shear layers have been undertaken (e.g., Lou et al. [12], Ameur and Chollet [13], and Nelson [14]). However, this study considers a wider range of convective Mach numbers for a fixed set of velocity and density ratios, so as to isolate compressibility effects. The velocity and density ratios for each case was specified as $u_2/u_1 = .164$ and

$\rho_2/\rho_1 = 3.33$. This density ratio corresponds to temperatures of $T_1 = 1000\ K$ and $T_2 = 300\ K$ at atmospheric conditions. For the high convective Mach number case, $M_1 = 2.41$ and $M_2 = .72$. The Mach numbers and temperature for this case roughly approximate the conditions of a nearfield missile exhaust plume shear layer for a low altitude trajectory condition. This high M_c case has been specifically chosen to approximate a missile plume to facilitate the development of RANS models for scalar fluctuations. These RANS models may then be used, for example, to make more reliable missile exhaust plumes predictions, as previously mentioned.

Progress toward the completion of the LES simulations for Part I of this study is currently limited to only the $M_c = 0.27$ and 1.3 cases. The $M_c = 0.8$ case has not yet been undertaken. For the $M_c = 1.3$ case, a full 3-D simulation has been completed. However, for the $M_c = 0.27$ case, only a 2-D simulation has been completed thus far. The lack of a full, 3-D simulation for the low speed case should not significantly degrade a preliminary assessment of compressibility effects because this case should be dominated by strong 2-D spanwise structures, with little contribution from 3-D effects to the mean scalar fluctuations. For example, several researchers have accurately reproduced the density fluctuations measured by Konrad for the Brown and Roshko [16] N_2/He shear layer using 2-D LES methodology.

The computational set-up for the $M_c = 0.27$ and 1.3 cases were different due to the Mach numbers involved. The low speed case used a rectangular domain .6 m in length along the streamwise coordinate. The computational domain was discretized using a $551x241$ grid. At the inflow boundary, hyperbolic tangent mean velocity and temperature profiles were specified using a characteristic subsonic boundary condition given the total temperature and mass flow rate. These profiles had a vorticity thickness of 7.3×10^{-3} m. The mean inflow profiles were also perturbed with sinusoidal streamwise velocity fluctuations at a 0.5 kHz frequency. For the high speed case, an additional upstream domain was added on the subsonic side to which total temperature and mass flow rate boundary conditions were applied. The multi-block grid for this case was ($551x100x65$, $28x47x65$). On the supersonic side, the mean velocity and temperature profiles were specified using a hyperbolic tangent profile with the same vorticity thickness. Sinusoidal forcing was applied to the transverse and spanwise velocity components at frequencies of 50, 100 and 200 kHz with phase angles that varied in the transverse direction and in time. A random component was also added to these velocity fluctuations.

4.0 Results and Discussion

Figure 1 presents contours of spanwise vorticity for both the low and high speed shear layer simulations. For the low speed case (Figure 1(a)), strong coherent structures are evident which pair and result in rapid shear layer growth.

These distinct structures are what may be expected for low speed shear layers as observed in the Brown and Roshko [16] N_2/He shear layer experiment. Also evident from this figure is the generation of vorticity due to baroclinic torque effects, which results from nonaligned density and pressure gradients. This may be seen by the large positive vorticity values primarily around the outer edges of the organized structures. For the high speed case (Figure 1(b)) the contours are quite different. As discussed by Sandham and Reynolds [9], at this high convective Mach number little or no coherent spanwise structures are readily apparent. This case shows a large amount of fine scale structure, which grows linearly in the downstream direction, as expected. From Figure 1(b), no well defined braid structures are apparent as seen in Figure 1(a). However, toward the end of the domain, there does appear to be the beginnings of large scale spanwise rotation of the fine scale structures, possibly resulting from the long delayed growth of the 2-D, spanwise modes.

For the high convective Mach number case, the flow is highly 3-D as seen in Figure 2, which presents a contour plot of the spanwise vorticity along several streamwise planes. This figure displays a flow rich in both small and large scale 3-D structure. The streamwise vorticity (Figure 3) also shows similar complexity. The 3-D structures seen in these figures were found to grow rapidly starting just shortly downstream of the shear layer origin. This is in agreement with the findings of linear stability analysis [9] for high convective Mach numbers that predicts 3-D modes to be amplified by a factor of five greater than 2-D modes.

The strong vortical features seen in Figures 1–3 result in complex scalar mixing patterns as seen in Figure 4. This figure presents temperature contours for both the low (Figure 4(a)) and high speed (Figure 4(b)) cases. For the low speed case, strong coherent structures with well defined braid regions (seen in Figure 1(a)) result in the penetration of hot fluid from the high speed side deep into the layer. The high speed case, with the lack of these well defined 2-D structures, exhibits a very different character. Large amounts of hot unmixed fluid are unable to traverse the layer before being mixed with surrounding fluid by the action of the fine scale structures. The highly complex mixing pattern associated with these fine scale 3-D structures may also be seen in Figure 5, which is a plot of temperature contours in several streamwise planes. Here again the highly complex mixing pattern is clearly evident. From both Figures 4 and 5, temperature overshoots above 1000 K on the high speed side are evident. These excess temperature regions result from compression waves, which move downstream with the vortical structures seen in Figure 1(b). These compression waves, and resulting temperature overshoots, are seen to persist the entire length of the layer, starting just downstream of the weak shock emanating from the inflow boundary. To facilitate direct comparison with Favre average RANS models, the LES data for these simulations are Favre time averaged assuming the

contribution from the subgrid is small. With these averaged data, relevant fluid dynamic quantities may be calculated, such as the streamwise evolution of the vorticity thickness (δ_ω).

Figure 6 presents a comparison of the vorticity thickness evolution for both cases. From this figure, both cases exhibit a linear growth regime downstream of ~ $x = 0.1$ m. The asymptotic growth rate for the high speed case is substantially lower than for the low speed case. This strong growth rate reduction is expected from the well known reduction of turbulent transport phenomenon with increasing compressibility. Within this linear region, the mean flow variable profiles are self-similar. For example, Figure 7 presents the Favre-averaged mean streamwise velocity profiles for both cases. The profiles in this figure are plotted against the transverse distance divided by the vorticity thickness. This is done to remove the growth rate difference seen in Figure 6. From Figure 7, there is clearly a shape change in the mean velocity with M_c. The high speed profiles have an anti-symmetric, hyperbolic tangent like profile. The low speed case, however, is not anti-symmetric and has a higher curvature on the high speed side. The source of this feature is unclear, but may be related to the baroclinic torque features seen in Figure 1(a).

Regarding the scalar property profiles, Figure 8 presents the Favre mean temperature in the linear growth regime. From this plot, first notice the 'hump' in the mean profile for the low speed case. This feature is characteristic of low speed, planar shear layers as observed by Friedler [15]. He suggested this feature was a result of the entrainment process associated with coherent, large scale spanwise structure characteristic of the low speed flow regime. As compressibility is increased and these spanwise structures disappear (Figure 1), this hump feature also disappears as seen for the high speed case. Figure 8 supports the suggestion that this hump feature is a result of the spanwise structures. Currently available RANS scalar transport models cannot capture this feature. Neither can the transition regarding compressibility be captured by current models. Time averaged transport data from these calculations will be used in Part II of this study to evaluate and improve RANS models for scalar transport to capture these features.

A further examination of Figure 8 suggest a dependence of turbulent Prandtl number on compressibility. Notice the low speed profile is considerably broader than for the high speed case. This difference is not a result of the growth rate difference between the two cases because this variation has been removed by normalization using the vorticity thickness. This difference suggests an increase in $\mathrm{Pr_t}$ with increasing compressibility. To make a preliminary assessment of this hypothesis, an estimate for $\mathrm{Pr_t}$ was made using the gradient hypothesis assumption, analogous to the eddy-viscosity, i.e.,

$$\nu_T = -\langle u'v' \rangle / (\partial \langle u \rangle / \partial y) \tag{3}$$

$$\alpha_T = \nu_T / \mathrm{Pr}_t = -\langle T'v' \rangle / (\partial \langle T \rangle / \partial y) \tag{4}$$

where the brackets (< >) represent Favre averaged quantities. Using Equations (3) and (4), Pr_t was constructed from the Favre average LES data. Figure 9 presents a plot of Pr_t across the layer of both cases. For the low speed case, Pr_t shows large variations and significantly lower values than for the high speed case over most of the layer. This drop in Pr_t implies a higher transport of temperature and hence a thicker temperature layer as seen in Figure 8. A similar observation was inferred by Sinha, et al. [6] for low speed jets. The high speed case, however, is more or less uniform across the layer with a value approaching the classic value of .9. This analysis supports the assertion that Pr_t increases with increased compressibility. This seems to be a significant finding regarding RANS modeling. However, this represents only a preliminary analysis and that will need to be borne out with further investigation.

Finally, Figure 10 presents the variation of rms temperature fluctuation intensity across the layer for the low and high speed cases. For the low speed case, the self-similar profile exhibits a double peak structure, while at high speeds the profile does not. This double peak structure for scalar fluctuations has been observed in the plane shear layer experiments of Friedler [15] and Brown and Roshko [16]. This feature is a common characteristic of low speed flows and results from the entrainment process involved with the large scale spanwise structures. Since the high speed case does not contain these structures, the profile only exhibits a single peak. This high speed profile is also thinner owing to the turbulent Prandtl number variation seen in Figure 9. Also observe the drop in peak intensity value as M_c is increased. The peak intensity drops by a factor of ~ .6 for the high speed case.

This reduction in peak intensity with increased compressibility is an interesting point in the context of the missile exhaust plume study of Calhoon and Kenzakowski [4]. In that study, a turbulent combustion model for RANS application was evaluated for the prediction of missile exhaust plume signatures. The combustion model used was strongly dependent on the prediction of temperature fluctuations from a modeled RANS transport equation. Due to the lack of available high speed data, this transport equation was calibrated based on available low speed data. Calhoon and Kenzakowski found this calibration to produce unrealistic results in the context of high speed missile exhaust plumes. To address this issue, the production coefficient in the temperature fluctuation transport equation was reduced to produce signatures consistent with flight data. This ad-hoc modification resulted in a reduction of the peak predicted temperature intensity values by a factor of ~ .75 below the low speed calibrated values. *It seems remarkable that this required reduction in predicted temperature intensity is in reasonable agreement with the reduction seen in Figure 10 resulting from compressibility effects.* The modeled fluctuation equation used by Calhoon and Kenzakowski did not include any validated model for compressibility, suggesting that the lack a compressibility correction was responsible for the observed error. This illustrates how LES may be used for the development of models to improve the prediction of production level codes. As

discussed earlier, Part II of this study will focus on the evaluation and development of RANS methodologies through the use of this LES data.

5.0 Conclusions

LES of hot planar shear layers have been carried out over a wide range of convective Mach numbers in order to assess the impact of compressibility effects on scalar fluctuations and turbulent transport. Simulations were completed for both low speed (M_c = .27) and high speed cases (M_c = 1.3). Analysis of the results leads to the following conclusions. In agreement with previous linear stability analysis, shear layer development from low compressibility to high compressibility is characterized by a transition from a flow dominated by coherent 2-D structures to one in which 3-D features dominate. This transition, or loss of 2-D structure, results in an evolution of mean scalar profiles that eliminates the 'hump' feature observed in low speed shear layer experiments. This transition also was found to modify the distribution of turbulent Prandtl number from a nonuniform profile at low speeds to an approximately uniform profile at high speed. This resulted in a smaller ratio of mean temperature profile width to vorticity thickness for the high speed case than for the low speed case. Also, the compressibility increase was found to modify the shape of the scalar fluctuation variation across the shear layer from a low speed two peak structure to a high speed single peak structure. This again is due to the reduction of 2-D structures in high speed shear layers. Finally, the identified reduction in peak temperature fluctuation values as compressibility was increased was found to be a credible explanation for the deficiencies of a RANS temperature fluctuation model applied to missile exhaust plume signature predictions in the study of Calhoon and Kenzakowski [4].

References

[1] Chien, K.Y., Ferguson, R.E., Kuhl, A.L., Glaz, H.M., and Collela, P., "Inviscid Dynamics of Two-Dimensional Shear Layers," 22nd AIAA Fluid Dynamics, Plasma Dynamics and Lasers Conference, Honolulu, HI, AIAA 91-1678, Jun. 24-26, 1991.

[2] Chidambaram N., Dash, S.M., and Kenzakowski, D.C., "Scalar Variance Transport in the Turbulence Modeling of Propulsive Jets," *Journal of Propulsion & Power*, Vol. 17, No. 1, Jan., Feb., 2001.

[3] Kenzakowski, D.C., Papp, J., and Dash, S.M., "Evaluation of Advanced Turbulence Models and Variable Prandtl/Schmidt Number Methodology for Propulsive Flows," AIAA Paper No. 2000-0885, 38th AIAA Aerospace Sciences Meeting at Reno, NV, Jan. 10–13, 2000.

[4] Calhoon, W.H. and Kenzakowski, D.C., "Flowfield and Radiation Analysis of Missile Exhaust Plumes Using a Turbulent-Chemistry Interaction Model," Paper No. AIAA-2000-3388, 36th AIAA/ASME/SAE/ASEE JPC and Exhibit, Von Braun Civic Center, Huntsville, AL, July 17–19, 2000.

[5] Sinha, N., Hosangadi, A., and Dash, S.M., "The CRAFT NS Code and Preliminary Applications to Steady/Unsteady Reacting, Multi-Phase Jet/Plume Flowfield Problems," CPIA Pub. 568, May 1991.

[6] Sinha, N., Lee, R., Dash, S.M., and Pelz, R.B., "Advances in 3D Unsteady Jet Simulation Using LES Methodology in a Parallel Environment," AIAA paper 96-1779, May 1996.
[7] Rai, M.M., "Navier-Stokes Simulations of Blade-Vortex Interaction Using High-Order Accurate Upwind Schemes," 25th AIAA Aerospace Sciences Meeting, Reno, NV, AIAA Paper 87-0543, Jan 12–15, 1987.
[8] Menon, S., "Active Control of Combustion Instability in a Ramjet Using Large-Eddy Simulations," 29th AIAA Aerospace Sciences Meeting, Reno, NV, AIAA Paper 91-0411, 1991.
[9] Sandham, N.D. and Reynolds, W.C., "Three-Dimensional Simulations of Large Eddies in the Compressible Mixing Layer," *J. Fluid Mech*, Vol. 224, pp. 133–158, 1991.
[10] Liu, X.-D., Osher, S., and Chan, T., "Weighted Essentially Non-oscillatory Schemes," *J. Comp. Phys.*, Vol. 115, pp. 220–212, 1994.
[11] Jameson, A., Schmidt, W., and Turkel, E., "Numerical Solutions of the Euler Equations by Finite Volume Methods Using Runge-Kutta Time-Stepping Schemes," presented at the AIAA 14th Fluid and Plasma Dynamics Conference, June 23–25, Palo Alto, CA, AIAA 81-1259, 1981.
[12] Liou, T.-M., Lien, W.-Y., and Hwang, P.-W., "Compressibility Effects and Mixing Enhancement in Turbulent Free Shear Flows," AIAA J, Vol. 33, No. 12, pp. 2332–2338, 1995.
[13] Ameur Si, M. and Chollet, J. P., "Large Eddy Simulations of Shear Flows: Mixing Layers," in *Advances in Turbulence*, V. Kluwer Acedemic Publishers, 1995.
[14] Nelson, C. C., "Simulations of Spatially Evolving Compressible Turbulence Using a Local Dynamic Subgrid Model," PhD thesis, Georgia Institute of Technology, 1997.
[15] Fiedler, H. E., "Transport of Heat Across a Plane Turbulent Mixing Layer," Advances in Geophysics, Vol. 18A, pp. 93–109, 1974.
[16] Brown, G. L. and Roshko, A., "On Density Effects and Large Structures in Turbulent Mixing Layers," *J. Fluid Mech*, Vol. 63, No. 2, pp. 775–816, 1972.

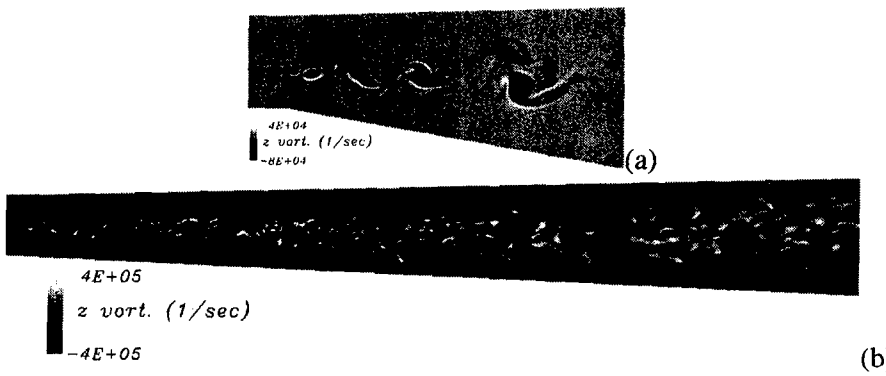

Fig. 1. Spanwise vorticity contours for (a) $M_c = .27$ and (b) $M_c = 1.3$. Flow is from left to right.

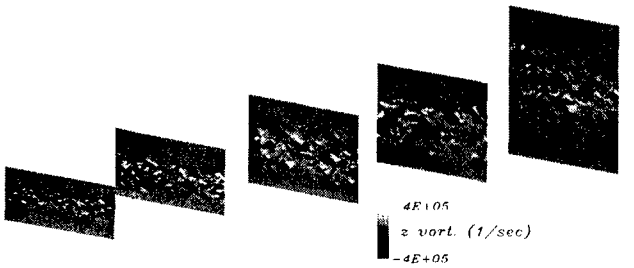

Fig. 2. Spanwise vorticity contours in streamwise planes for the $M_c = 1.3$ case.

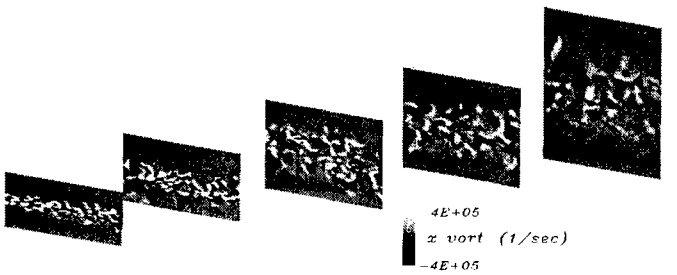

Fig. 3. Streamwise vorticity contours in streamwise planes for the $M_c = 1.3$ case.

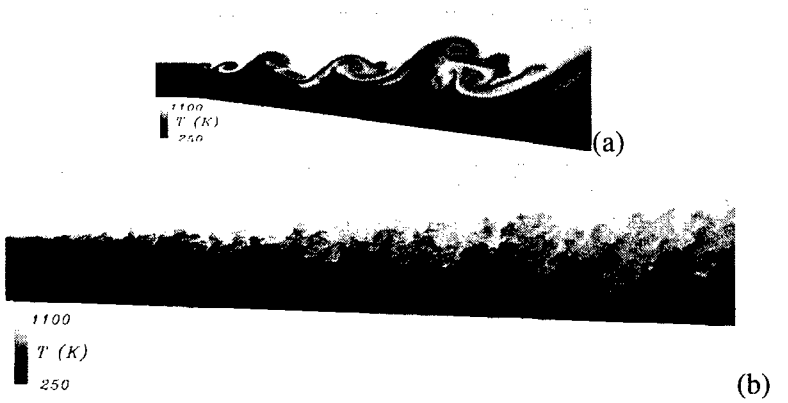

Fig. 4. Temperature contours in a spanwise plane for (a) $M_c = .27$ and (b) $M_c = 1.3$.

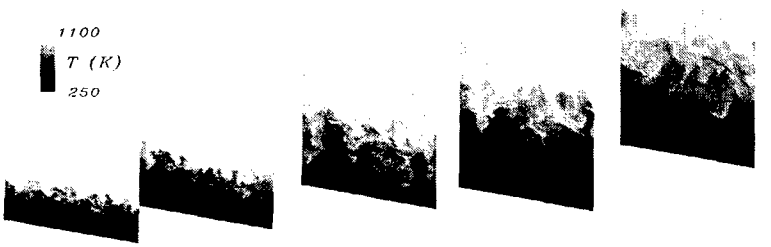

Fig. 5. Temperature contours for $M_c = 1.3$ at several streamwise planes.

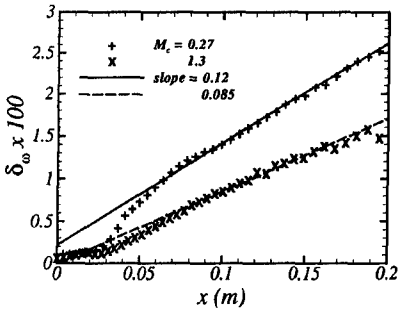

Fig. 6. Vorticity thickness evolution as function of downstream distance.

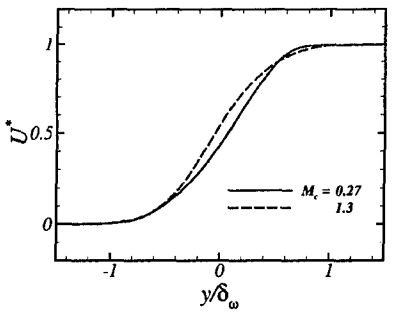

Fig. 7. Favre mean normalized streamwise velocity in the linear growth rate regime for the low and high speed cases.

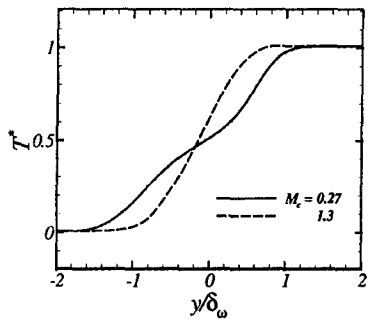

Fig. 8. Favre mean normalized temperature profiles in the linear growth rate regime.

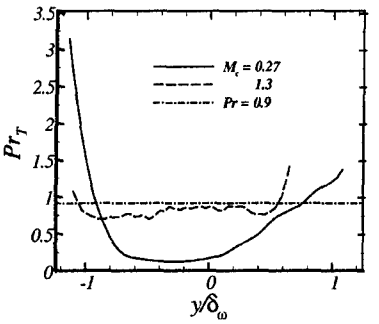

Fig. 9. Estimated turbulent Prandtl number variation across the shear layer for the low and high speed cases.

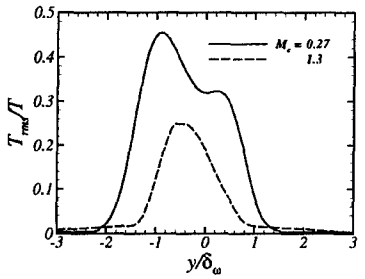

Fig. 10. Shear layer temperature intensity variation for the low and high speed cases.